UNIVERSITY OF PADUA, DEPARTMENT OF INFORMATION ENGINEERING

- Imaging for Neuroscience -
Homework 3: DMRI/fMRI Integration

Giulia Bressan, ID 1206752

A.Y. 2019/2020

INTRODUCTION

The aim of the study is to investigate the relationship between the resting state fMRI analysis and the diffusion MRI data.
This work and the related code is organized in three sections, as follows:

1. Resting state fMRI analysis;
2. Diffusion MRI analysis;
3. DMRI/fMRI integration.

Each section contains various assignments, each of which will be briefly explained and commented in this report. The data used to perform the analysis were scans collected in Verona and acquired with a 3T MR scanner on a healthy subject.

1 RESTING STATE FMRI ANALYSIS

The first part of the assignment is related to the analysis of fMRI data and consists of seven tasks:

1. Data preprocessing;
2. Data denoising;
3. Volume censoring;
4. Check of preprocessing step;
5. Static FC matrix computation;
6. Multiple Comparison Correction;
7. Graph measures.

1.1 Data preprocessing

The first task performed during the data preprocessing was the segmentation of the T1w structural image into White Matter (WM), Grey Matter (GM) and Cerebro-Spinal Fluid (CSF). This was done using the SPM sotware of Matlab. In this way we obtained the three tissues probability maps, each indicating the probability of one voxel to belong to WM, GM or CSF, respectively.
Then we thresholded the maps in order to obtain the masks for each of the tissues. In Table 1.1 the selected thresholds are shown. We chose the values by visually inspecting the resulting masks, keeping the regions we were interested in and discarding the other areas. We then eroded the three masks using a customized structuring element with shape [1; 1], as we saw that preserving the horizontal component was better for the final result, and the structuring elements provided by the Matlab function were too aggressive in the filtering. In Figure 1.1 the original maps and the obtained masks are shown.

Map	Value of the threshold
GM	0.9
WM	0.9
CSF	0.8

Table 1.1: Values of the threshold.

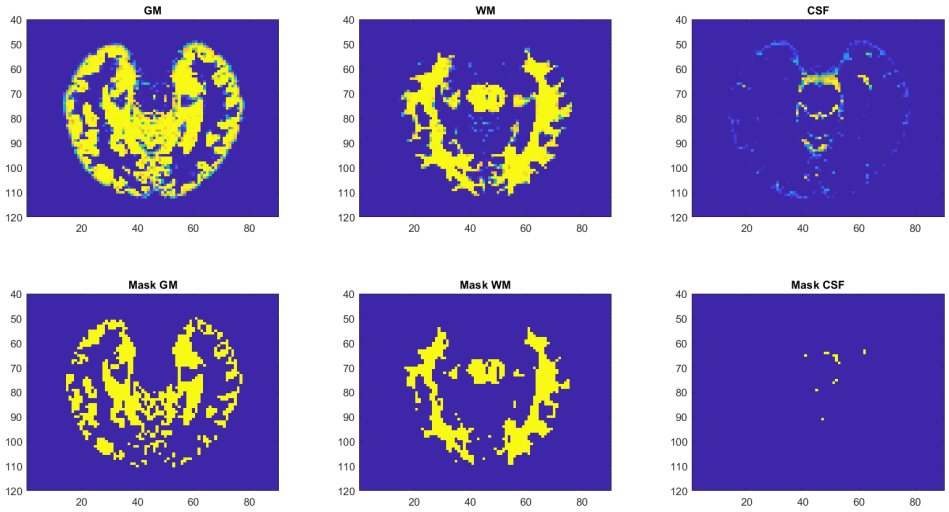

Figure 1.1: Assial view of original maps (top) and derived masks (bottom) [Slice 45].

After that, we computed the mean fMRI signal of WM and CSF.
Then, we created the sumEPI image and we defined a mask for this image as well. The threshold was fixed by visually inspecting the histogram of the image and the final result, which had to consider the entire brain while discarding the possible noise created around it during acquisition. The chosen value was of 0.75e7. Since given that threshold there was more than one connected component, we applied a procedure for keeping just the biggest one, corresponding to the brain region, while discarding the others. The result is shown in Figure 1.2.

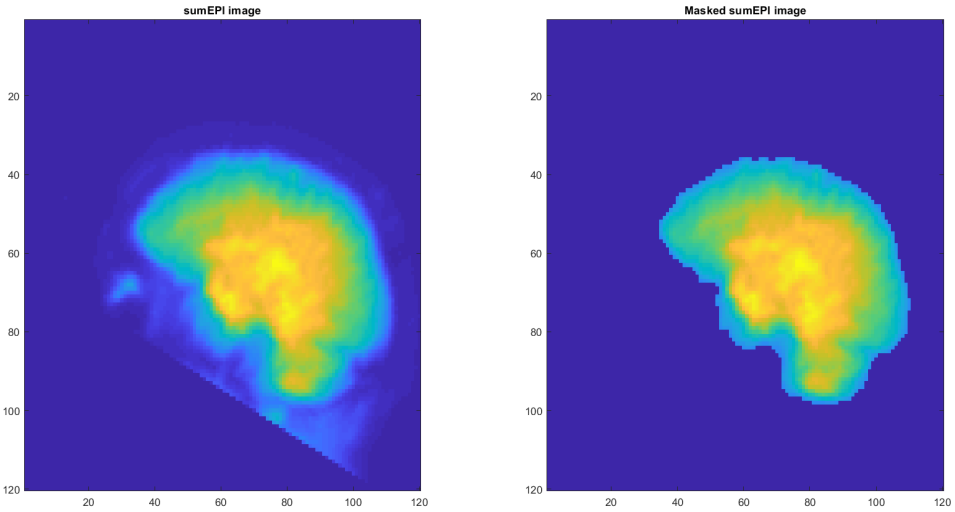

Figure 1.2: Sagittal view of SumEPI image and relative mask.

The masks of GM and sumEPI were then used to mask the Hammer Atlas, in order to be able to subsequently perform the ROIs time activity curve extraction: after discarding the ROIs with less then 10 voxels and those belonging from amygdala, cerebellum, brainstem, corpus callosum, substantia nigra and ventricles, we computed the mean fMRI signal for each masked ROI of the atlas.

1.2 Data denoising

First, from each ROI we removed the non-neural undesired fluctuations from the temporal dynamic, using a linear regression approach. Each regressor had to be converted to z-scores before being used. In Figure 1.3 the obtained regression matrix is shown.

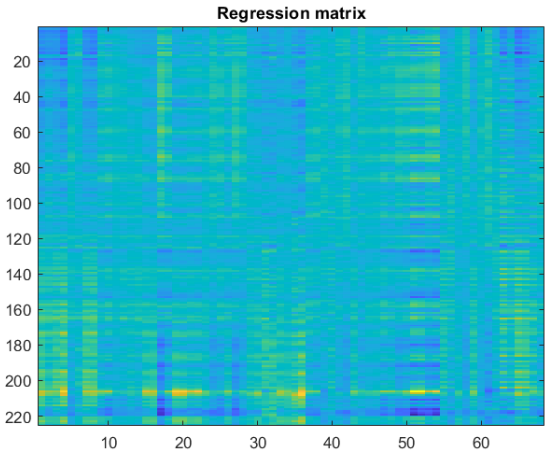

Figure 1.3: Regression matrix (with regressors converted to z-scores).

Then, in order to take the slow components of the signal out, we filtered the denoised signal with an high-pass filter with cut-off frequency equal to $1/128$ Hz (which is a standard choice for the cut-off frequency, also used in the SPM software).

1.3 Volume censoring

The next step was to discard the volumes that were affected by motion artefacts. In order to do so, we checked if in the given Framewise Displacements (FD) matrix the values of the first column were bigger than 3.5 mm. As it was not the case, we did not discard any volume, since they did not present significative motion artefacts.

1.4 Check of preprocessing step

To check the quality of the preprocessing applied to the signals, we plotted the time course of the right hippocampus region (region 1 in the Hammer Atlas), before any preprocessing and after each step. As we can see in Figure 1.4, the original signal had a drift from the baseline, that was removed after the denoising step. The high-pass filtering was then able to remove the slow fluctuations of the signal, that remained after the denoising.

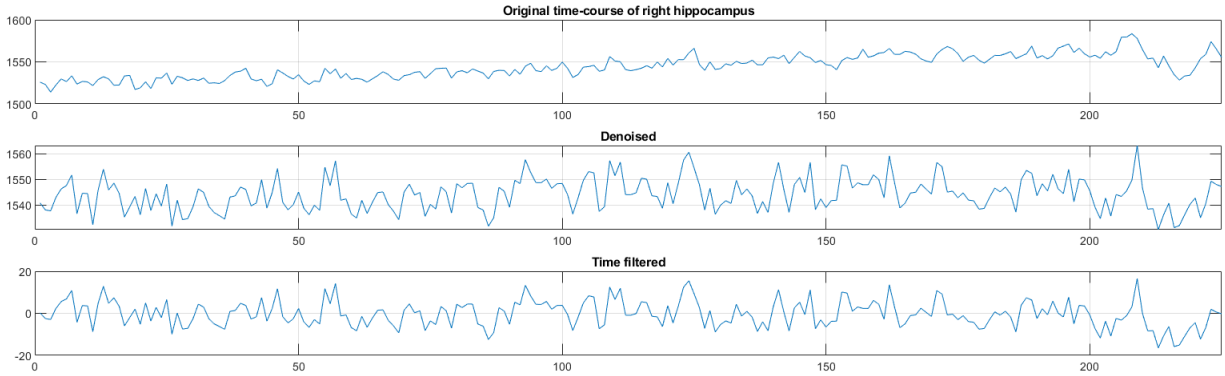

Figure 1.4: Original time-course of the right hippocampus region and signals obtained after each denoising step.

1.5 Static FC matrix computation

In this step we computed the pairwise Pearson's correlation between the time-series of the ROIs, in order to check whether there was correlation between the neural activity in different brain regions. In Figure 1.5 the Functional Connectivity (FC) matrix is shown, and we can see the higher values of connectivity in the more yellow areas (except for the principal diagonal were we have the autocorrelation).

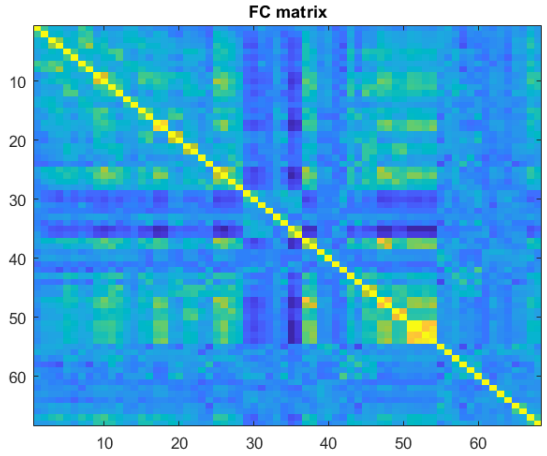

Figure 1.5: FC matrix (after applying the Fisher's z-transform to the coefficients).

1.6 Multiple comparison correction

We then performed a multiple comparison correction, using a False Discovery Rate (FDR) approach with significance level $\alpha = 0.05$. We chose this method over the Bonferroni approach as we know that Bonferroni is usually overly conservative and it also assumes that all tests are independent, while in fMRI we have spatial autocorrelation, as data from one voxel are correlated with data from the neighbouring ones. The obtained result was of 2470 significant tests, out of 4624 (as we had 68 ROIs to analyse).

1.7 Graph measures

The last task to perform for the fMRI analysis was the computation of some metrics to summarize the functional connectivity in terms of node centrality. We computed the node degree, strength and the normalized betweenness centrality, considering only the functional connections that resulted as significative after the multiple comparison correction step. In Figure 1.6 the obtained values are shown, along with the ROIs that reached the highest 10 values for each metric. The indices of these regions are also reported in Table 1.2.

Metric	Indices of top 10 ROIs
Node degree	5 10 11 25 26 27 37 38 47 67
Node strength	10 11 25 26 37 38 47 48 51 52
Normalized betweenness centrality	17 25 26 29 30 34 35 36 47 55

Table 1.2: Top 10 ROIs with highest measures of centrality.

2 Diffusion MRI analysis

The second part of the assignment is related to the analysis of Diffusion MRI data and consists of two tasks:

1. Diffusion signal visualization and understanding;
2. Diffusion tensor computation.

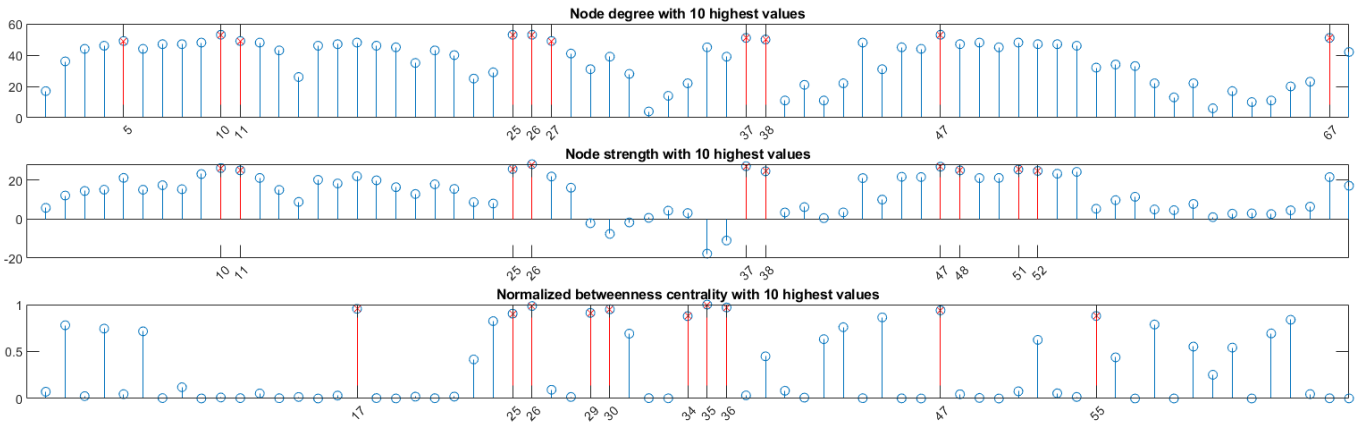

Figure 1.6: Node degree, node strength and normalized betweenness centrality, with top 10 values in red.

2.1 Diffusion signal visualization and understanding

After loading the diffusion data, we analysed them in terms of number of DWIs and shells acquired. The different shells were considered with a tolerance of $\alpha = \pm 20 s/mm^2$. The result was of two different shells, at $700 s/mm^2$ and $2000 s/mm^2$, plus the one with b=0, with an acquisition of 103 DWIs.
In order to find a voxel populated principally with CSF, we looked at the Fractional Anisotropy (FA) values, computed later, and we chose a voxel for which its value was close to zero, since it corresponds to isotropic movements of water molecules, which is the case of the CSF. In Figure 2.1 the diffusion signal unsorted and ordered by its b-value is shown. By visually inspecting it we can see some intra b-value variability, with a slight increase with higher b-values, probably due to some noise in the acquisition, as increasing the b-value the SNR is reduced. The inter b-value variability can be seen from the "steps" that the signal forms, more visible in the sorted one: for smaller b-value the signal is higher, and we can also see that the diffusion time is higher.

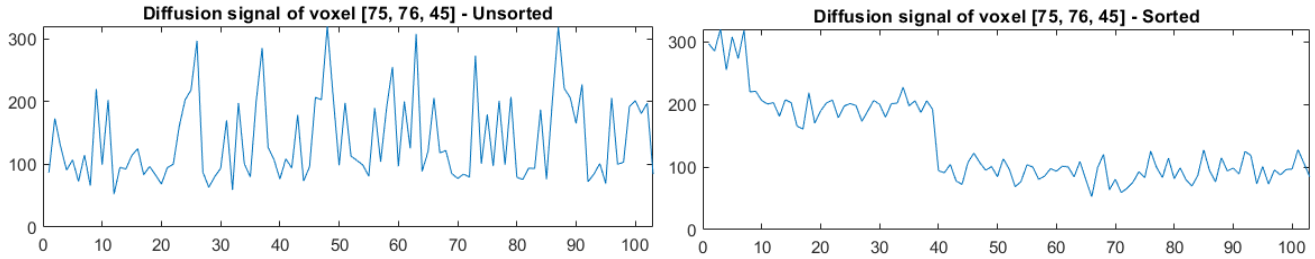

Figure 2.1: Diffusion signal of a voxel populated mainly with CSF, unsorted (left) and sorted (right) by its b-value.

2.2 Diffusion tensor computation

In order to fit the voxel-wise diffusion tensor, we first created two new 4D matrix, one containing only the volumes corresponding to $b = 0 s/mm^2$ (used to compute S0) and the other with also the shell closest to $b = 1000 s/mm^2$ previously identified. We then fitted the voxel-wise diffusion tensor using a linear least squares approach, in two different ways. For the first one (referred as 2b) we computed S0 using the voxel-wise value of the first $b = 0$ volume of the available dataset, while for the second (referred as 2c) we used as S0 the voxel-wise mean value of all $b = 0$ volumes. We recovered the FA and Mean Diffusivity (MD) indexes using the eigenvalue/eigenvector decomposition and then we computed the voxel-wise coefficients of variation (CV) for both of the indexes, with the following formula (same for MD):

$$CV_{voxel} = 100 * \frac{FA_{mean} - FA_{voxel}}{FA_{mean}}$$

In Figure 2.2 the four different maps are shown. Looking at the plot of the mean difference (not reported here) of the CVs computed with the two different approaches, we can see that the FA index seems in general more affected

by the different normalization choice, but this may vary from slice to slice (in fact, in Figure 2.2 for slice 72 the MD index seems the one changing more).

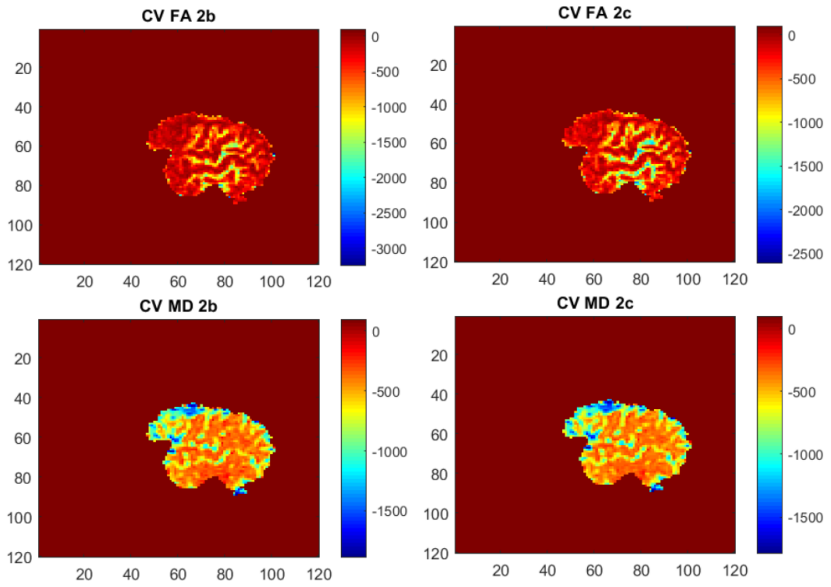

Figure 2.2: Sagittal view of the CVs images for FA (top) and MD (bottom), for the two different approaches (slice 72).

Out of the two different diffusion tensors fitted, we decided to keep the ones computed with S0 as the voxel-wise mean value of all $b = 0$ volumes, as we thought that the estimation obtained using the mean of multiple values would be more accurate than using a single value for S0. Also, looking at the CVs we could not discriminate for the best approach, as the mean values of the CVs were almost the same for the two approaches. The visualization of the two chosen maps is reported in Figure 2.3.

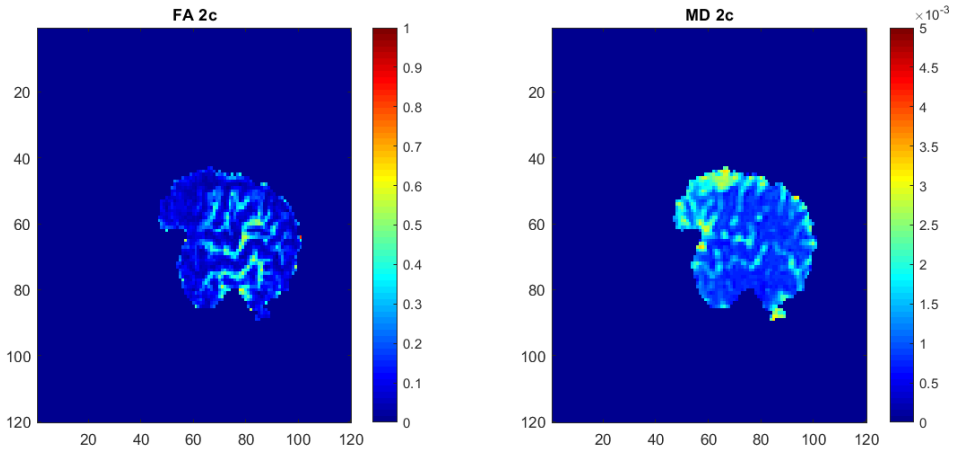

Figure 2.3: Sagittal view of the FA and MD maps of the chosen approach (slice 72).

Then we masked the FA and MD maps with the masks obtained in Section 1 (GM mask and sumEPI mask), as we previously did for the Hammer Atlas. Finally, we computed their mean value in each ROI.

3 DMRI/FMRI INTEGRATION

The last part of the assignment concerns the integration of the results obtained from the fMRI and DMRI analyses and it is divided in two parts:

1. Visual inspection;
2. Quantitative results.

3.1 Visual inspection

In this section the scatterplots of the three metrics computed in Subsection 1.7 versus the ROIs FA and MD (computed in Subsection 2.2) are plotted. Figure 3.1 shows the obtained plots, along with the linear fitting of the data, to show the general behaviour of the data correlation.

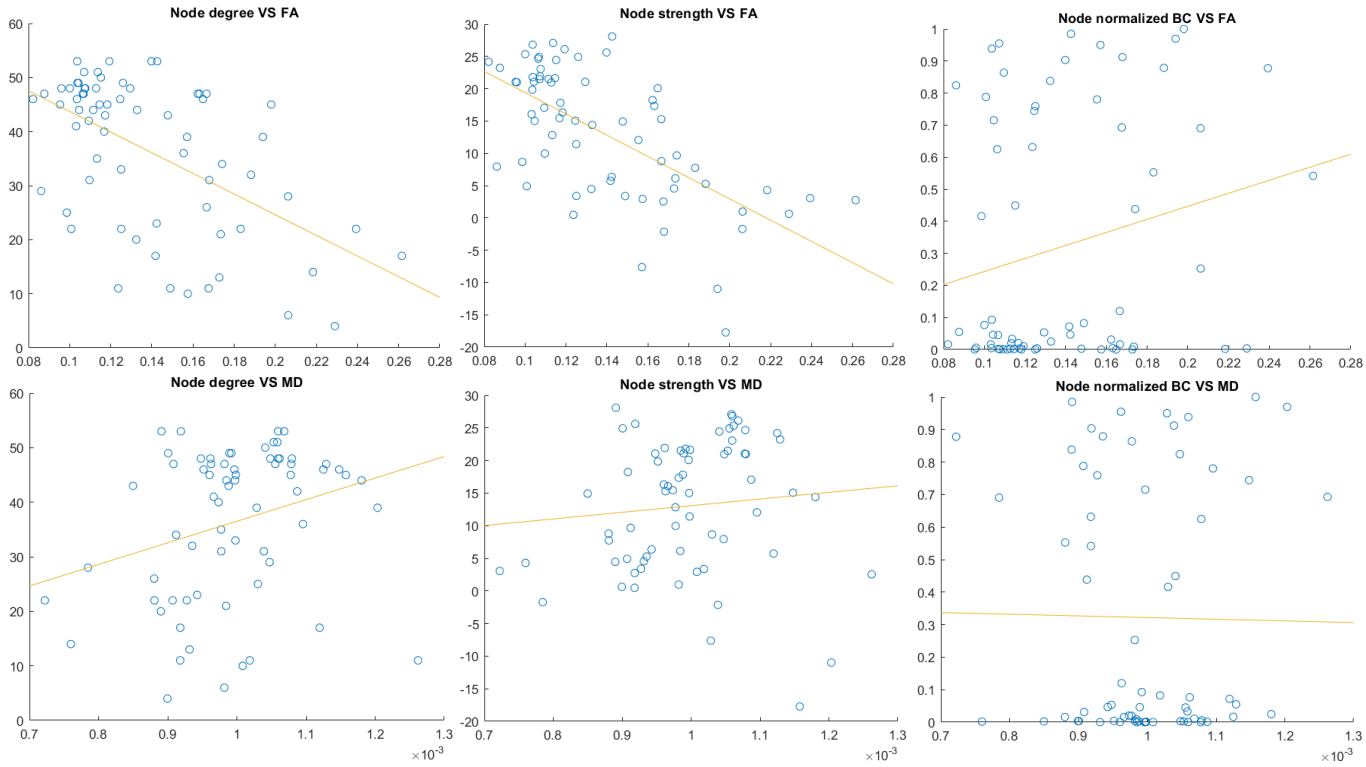

Figure 3.1: Scatterplot of ROIs node degree, strength and normalized betweenness centrality, in the y-axes, versus ROIs FA and MD, in the x-axes (from left to right and from top to bottom, respectively).

3.2 Quantitative results

Finally, we computed the Pearson's correlation between the six pairs of variables of Subsection 3.1. The results are shown in Table 3.1.

VS	FA	MD
Node degree	-0.5475	0.2805
Node strength	-0.6456	0.0989
Normalized betweenness centrality	0.2130	-0.0133

Table 3.1: Pearson's correlation between the six pairs of variables.

We can see that there is an inverse correlation between node degree and node strength and the FA index. This is in accordance with the results of the scatterplots in Figure 3.1, where the linear interpolation clearly shows that a decrease in the node degree and node strength values corresponds to the increase of the FA index. Node degree has also a slight direct correlation with MD, while node strength seems to be quite uncorrelated with MD. The normalized betweenness centrality, then, has a low direct correlation with the FA index, and it seems uncorrelated with MD.